Fines-controlled drainage in just-saturated, inertial column collapses

William Webb[1*], *Charles* Heron[1], and *Barbara* Turnbull[1]

[1]Faculty of Engineering, University of Nottingham, Nottingham, NG7 2RD, UK

Abstract. The wide particle size distributions, over several orders of magnitude, observed in debris flows leads to a diverse range of rheological behaviours controlling flow outcomes. This study explores the influence of different scale grains by conducting subaerial, fully saturated granular column collapse experiments with extreme, bimodal particle size distributions. The primary particles were of a size where their behaviour was controlled by their inertia while a suspension of kaolin clay particles within the fluid phase acts at spatial scales smaller than the pore space between the primary particles. The use of a geotechnical centrifuge allowed for the systematic variation of gravitational acceleration, inertial particle size and the degree of kaolin fines. Characteristic velocity- and time-scales of the acceleration phase of the collapse were quantified using high-speed cameras. Comparing tests containing fines to equivalent collapses with a glycerol solution mimicking the enhanced viscosity but not the particle behaviour of the fines, it was found that all characteristic dynamic quantities were dependent on the degree of fines, the system size, the grain fluid-density ratio and the column– and grain-scale Bond and Capillary numbers. We introduce a fine-scale Capillary number showing that, although surface tension effects at the column scale are negligible, fines do control the movement of fluid through the pore spaces.

1 Introduction

The influence of a wide particle size distribution on the dynamics and outcomes of naturally occurring debris flows is still disputed. Field studies [e.g. 1] and large-scale testing [e.g. 2] have shown that events containing high quantities of fine granular material, like clays and silts, often achieve increased mobility through the development of significant excess pore pressures which reduce the frictional energy losses between the bulk flow and the terrain bed.

Recent two-phase shallow water models [3-5] have attempted to capture the temporal and spatial variation of the grain size distribution by modelling aspects of unsteady debris flow behaviour. However, there is still no consensus on the most appropriate, computationally efficient way to implement this complexity. This suggests that a more refined understanding of the mechanisms controlling grain-scale flow dynamics is required to allow conclusions to be made on what physical processes are most influential on global flow outcomes.

Given the small length and time scales associated with these effects, it seems pertinent to analyse them further by conducting laboratory-scale experiments where it is possible to fully control the initial and boundary conditions of the flow [6]. A notable study [7] utilised a drum centrifuge configuration to evaluate the influence of the particle size distribution on steady-state flow dynamics. They found that mixtures that contained higher percentages of fine granular material exhibited more significant and prolonged excess pore pressures which reduced bulk flow resistance. While this is encouraging, further parametric investigations are required to quantitatively evaluate the influence of the inclusion of fines on flow dynamics and understand the mechanisms at play.

A recent study [8] attempted to isolate the influence of inertial grains on flow dynamics over a wide parameter space by conducting g-elevated, fluid-saturated granular column collapse experiments where water-glycerol mixtures were used as a pseudo-fluid. The current study attempts to build on this work and introduce an extreme bimodal grain size distribution by using a fluid phase comprised of kaolin clay particles and water. As such, by varying gravitational acceleration, the coarse grain diameter and the percentage of fines, the influence of the fine length- and time-scales on acceleration phase collapse dynamics is evaluated and compared within the previously established parameter space.

2 Methodology

2.1 Experimental setup

The experiment (see Figure 1) consists of rapidly releasing a granular-fluid mixture, which is initially accommodated within a partially filled steel cylinder, over a horizontal plane where it is allowed to spread under the influence of a prescribed gravitational acceleration G. By spinning the apparatus at the end of a geotechnical beam centrifuge, the collapse can occur at an elevated

* Corresponding author: evyww@nottingham.ac.uk

gravitational acceleration $G = Ng$ where N is dependent on the effective radius and rotational speed of the model, and $g = 9.81$ m s^{-2}.

The current study focused on the collapse of fluid saturated granular columns with an initial height H_0 = 50 mm and a column radius $r_0 = 54$ mm. The granular phase was comprised of soda lime glass spheres with a density $\rho_p = 2642 \pm 27.4$ kg m^{-3} and a mean packing fraction $\phi_p = 0.61 \pm 0.01$. The fluid phase consisted of kaolin clay particles suspended in water. Tests were conducted over a wide parameter space by varying $G =$ [9.81, 45.22, 137.64, 275.45] m s^{-2}, the coarse grain diameter $d_p =$ [4, 8] mm, and the degree of fines suspended within the fluid by mass $C_k =$ [0.1, 0.2]. Assuming a characteristic collapse strain rate $\gamma = \sqrt{G/H_0}$, the density, viscosity and surface tension of the fluid phase was varied between $\rho_s =$ [1165, 1330] kg m^{-3}, $\mu_s =$ [7.65, 108.30] cP, and $\sigma_s =$ [92.59, 98.96] mN m^{-1}, respectively.

The evolution of the collapsing mixture was recorded by two Go-Pro cameras and the temporal evolution of the collapse front was obtained through the image analysis procedure detailed in [8].

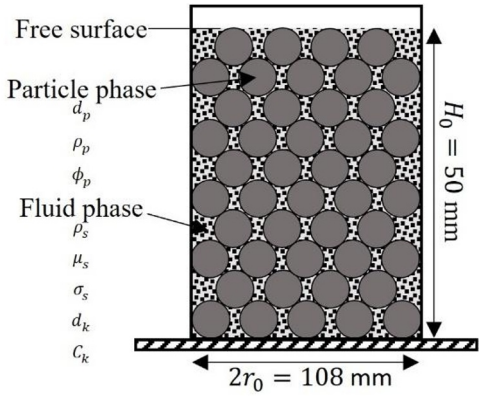

Fig. 1. Schematic of the initial column configuration prior to collapse initiation.

2.2 Dimensional analysis

Buckingham's Π theorem [9] can be used to examine how different test parameters may impact the propagation of the collapse. As such, a relationship between the flow front velocity u at time t with the collapse test parameters can be hypothesised as

$$u = f_1\left(H_0, r_0, d_p, \rho_p, \phi_p, C_k, d_k, \rho_s, \mu_s, \sigma_s, t, G\right) \quad (1)$$

where f_1 is an unknown function and d_k is a reference length scale for the kaolin clay particles taken as 5 μm. The theorem then states that the 11 dimensional quantities in Equation (1), which are functions of mass, length and time scales, can be interrelated by 8 dimensionless Π-groups. Following the methodology described in [10], Equation (1) can be transformed into the following form

$$\frac{u}{\sqrt{GL}} = f_2\left(\phi_p, C_k, \frac{r_0}{d_p}, \frac{t}{\sqrt{LG^{-1}}}, \frac{(\rho_p-\rho_s)N}{\rho_s}, \frac{\rho G d_p H_0}{\sigma_s}, \frac{\rho G d_p d_k}{\sigma_s}, \frac{\mu_s\sqrt{GH_0^3}}{\sigma_s d_p}, \frac{\mu_s\sqrt{Gd_p^3}}{\sigma_s d_k}\right) \quad (2)$$

where f_2 is an unknown function, L is the characteristic length scale of interest and ρ is the granular-fluid mixture effective density $\rho = \phi_p\rho_p + (1-\phi_p)\rho_s$. The parameter on the left-hand side of Equation (2) is the flow front Froude number Fr_L which is the ratio of inertial and gravitational forces over a characteristic length scale L. The first two parameters on the right-hand side of Equation (2) are the dimensionless parameters ϕ_p and C_k which remain unchanged from Equation (1). The third parameter, r^* is the ratio between r_0 and d_p. The fourth parameter, t^*, compares t against the length scale dependent characteristic inertial timescale $\sqrt{LG^{-1}}$. The fifth parameter is the relative granular-fluid density ratio accounting for acceleration-scale buoyancy effects ρ^*. The sixth and seventh parameters are referred to as the column- and grain-scale Bond numbers, Bo and Bo_k , respectively. The first parameter quantifies the relative influence of inertial forces at the column scale against capillary forces at the grain scale while the latter is an analogous quantity relating grain scale inertial forces to kaolin scale capillary effects. The final two parameters are scale-relative Capillary numbers. The first relates column scale viscous forces to grain scale capillary effects Ca while the second compares grain scale viscous forces to kaolin scale capillary effects Ca_k.

As stated in [10], given that Π groups can be recast through multiplication, the dimensionless parameter set in Equation 2 is not a unique solution to Equation (1). This set was deemed suitable as it has significant overlap with the dimensionless set used in the previous scale analysis study [8]. The included force ratio terms also allow for comparison across all three length scales of interest (H_0, d_p and d_k) which is critical in interpreting the contribution of the fine particulate to flow dynamics throughout the acceleration phase.

3 Results and Discussion

The acceleration phase of each collapse was characterised by the maximum velocity of the flow front u_m, and the time elapsed between collapse initiation and the instance where u_m was achieved t_m. The two camera angles allowed averaged values of the two quantities to be taken which reduces the impact of external forces resulting from centrifuge modelling like the Coriolis force.

Given that ϕ_p remains approximately constant across all tests, Equation (2) can be simplified as follows

$$\mathrm{Fr}_{m,L} = f_3\left(C_k, r^*, t^*_{m,L}, \rho^*, \mathrm{Bo}, \mathrm{Bo}_k, \mathrm{Ca}, \mathrm{Ca}_k\right) \quad (3)$$

where $\mathrm{Fr}_{\mathrm{m,L}}$ and $t^*_{m,L}$ are equivalent to Fr_{L} and t^*_L evaluated at u_m and t_m, respectively. The characteristic length scales of interest L are d_p and H_0 meaning that there are four quantities of interest Q related to the acceleration phase of the collapse; Fr_{m,d_p}, Fr_{m,H_0}, t^*_{m,d_p}, and t^*_{m,H_0}.

To evaluate the effect of the inclusion of fines on the acceleration phase, a single dataset containing the quantities collected from the current study and the same

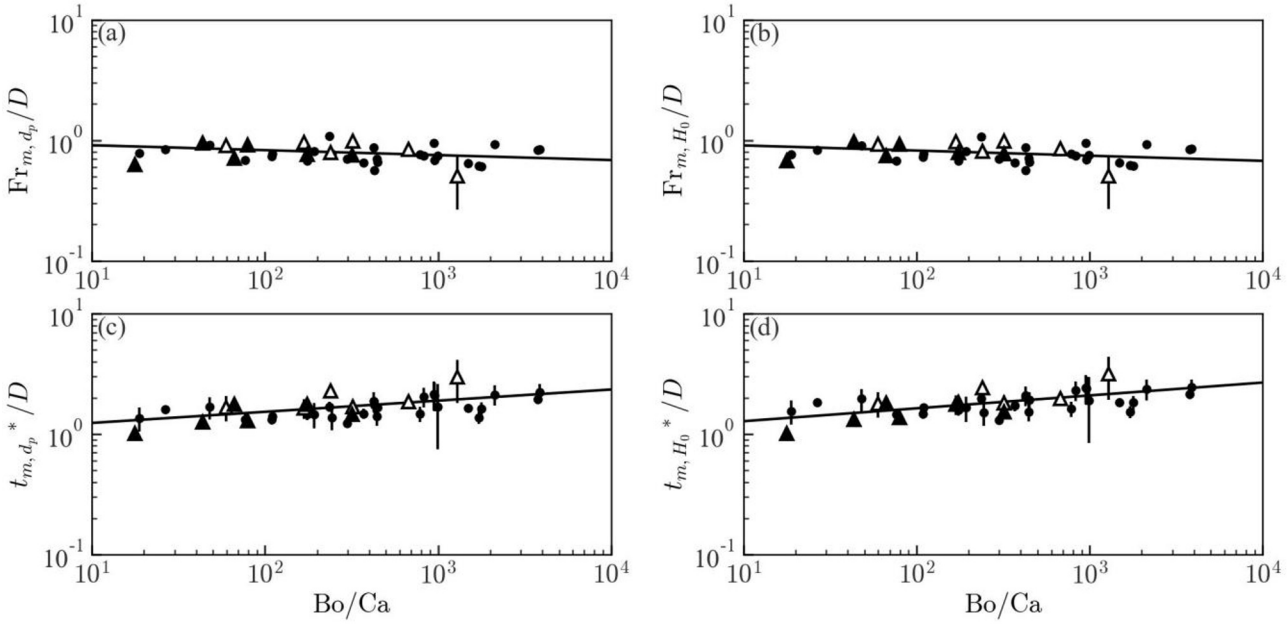

Fig. 2. (a) $\mathbf{Fr}_{m,d_p}$, **(b)** $\mathbf{Fr}_{m,H_0}$, **(c)** $\boldsymbol{t}_{m,d_p}$ and, **(d)** $\boldsymbol{t}_{m,H_0}$ normalised by $\boldsymbol{D} = \left(\frac{\mathbf{Bo}_k}{\mathbf{Ca}_k}\right)^{k_2 C_k} (\mathbf{Ca}_k)^{k_3 C_k} (\boldsymbol{\rho}^*)^{k_4} (\boldsymbol{r}^*)^{k_5}$ against $\mathbf{Bo/Ca}$ for $\boldsymbol{C_k} =$ 0 (●), $\boldsymbol{C_k} = 0.1$ (△) and $\boldsymbol{C_k} = 0.2$ (▲). The black line defines the power law fit described by Equation (4) using the exponents provided in Table (1). Error bars define the absolute error of the independent variable.

quantities published in [8] for the Newtonian fluid test cases, where $C_k = 0$, and Bo_k and Ca_k values are not considered, was developed. The influence of every parameter in Equation (3) was then evaluated using a non-linear regression scheme and, as was found for the Newtonian fluid dataset, the measured quantities of interest can be described by empirical power law fits that are independent of the other quantities of interest. For the current combined dataset, this relationship is defined as

$$Q = \left(\frac{\mathrm{Bo}}{\mathrm{Ca}}\right)^{k_1} \left(\frac{\mathrm{Bo}_k}{\mathrm{Ca}_k}\right)^{k_2 C_k} (\mathrm{Ca}_k)^{k_3 C_k} (\rho^*)^{k_4} (r^*)^{k_5} \quad (4)$$

where k_1 – k_5 are constants summarised in Table 1. Figure 2 details the finalised fits for each Q. The structure of Equation (4) allows Newtonian- and non-Newtonian-fluid tests to be fitted to the same power law as terms that include parameters associated with the kaolin-scale can be neglected as $C_k = 0$.

Equation (4) is very similar in structure to the empirical fit found for Q in the case of the purely Newtonian fluid dataset

$$Q = \left(\frac{\mathrm{Bo}}{\mathrm{Ca}}\right)^{\alpha} (\rho^*)^{\beta} (r^*)^{\gamma} \quad (5)$$

where α, β, and γ are constants. It is reassuring to see that the general trend and, the coefficients of the terms that are independent of kaolin-scale phenomena (i.e. k_1, k_4 and k_5), are largely comparable in both magnitude and sign for Equation (4) and Equation (5) for all Q. The normalised root mean squared error $\mathrm{RMSE_N}$ has also reduced for every Q.

The most significant outcome from this study is the appearance of the Ca_k term in Equation (4). This suggests that the inclusion of fine granular material results in all acceleration phase quantities of interest being dependent on surface-tension effects emanating from the kaolin-scale. In contrast, as demonstrated by Equation (5), surface tension effects were not pertinent to the behaviour of the Newtonian fluid test case.

Table 1. Summary of exponents for Equation (4) for all Q along with the normalised root mean squared error $\mathrm{RMSE_N}$ of each fit.

	$\mathbf{Fr}_{m,d_p}$	$\mathbf{Fr}_{m,H_0}$	$\boldsymbol{t}^*_{m,d_p}$	$\boldsymbol{t}^*_{m,H_0}$
$\boldsymbol{k_1}$	-0.04	-0.04	0.09	0.11
$\boldsymbol{k_2}$	0.07	0.15	-0.48	-0.63
$\boldsymbol{k_3}$	0.18	0.27	-0.40	-0.55
$\boldsymbol{k_4}$	0.10	0.11	0.22	0.23
$\boldsymbol{k_5}$	0.30	-0.19	-0.48	-0.07
$\mathbf{RMSE_N}$	0.14	0.19	0.11	0.10

The relative importance of each force ratio term in Equation (4) associated with the grain- and kaolin-length scales can be quantified by comparing their magnitude and sign to the magnitude and sign of $(\mathrm{Bo/Ca})^{k_1}$. Figure (3) shows the plots of $(\mathrm{Bo}_k/\mathrm{Ca}_k)^{C_k k_2} (\mathrm{Bo/Ca})^{-k_1}$, $(\mathrm{Ca}_k)^{C_k k_3} (\mathrm{Bo/Ca})^{-k_1}$ and $(\mathrm{Bo}_k/\mathrm{Ca}_k)^{C_k k_3} (\mathrm{Bo}_k/\mathrm{Ca}_k)^{-C_k k_2}$ against $\mathrm{Bo/Ca}$ for $\mathrm{Fr}_{m,L}$ and $t^*_{m,L}$. The figure shows that for $\mathrm{Fr}_{m,L}$ and $t^*_{m,L}$, the trend for both characteristic length scales is similar for all values of C_k.

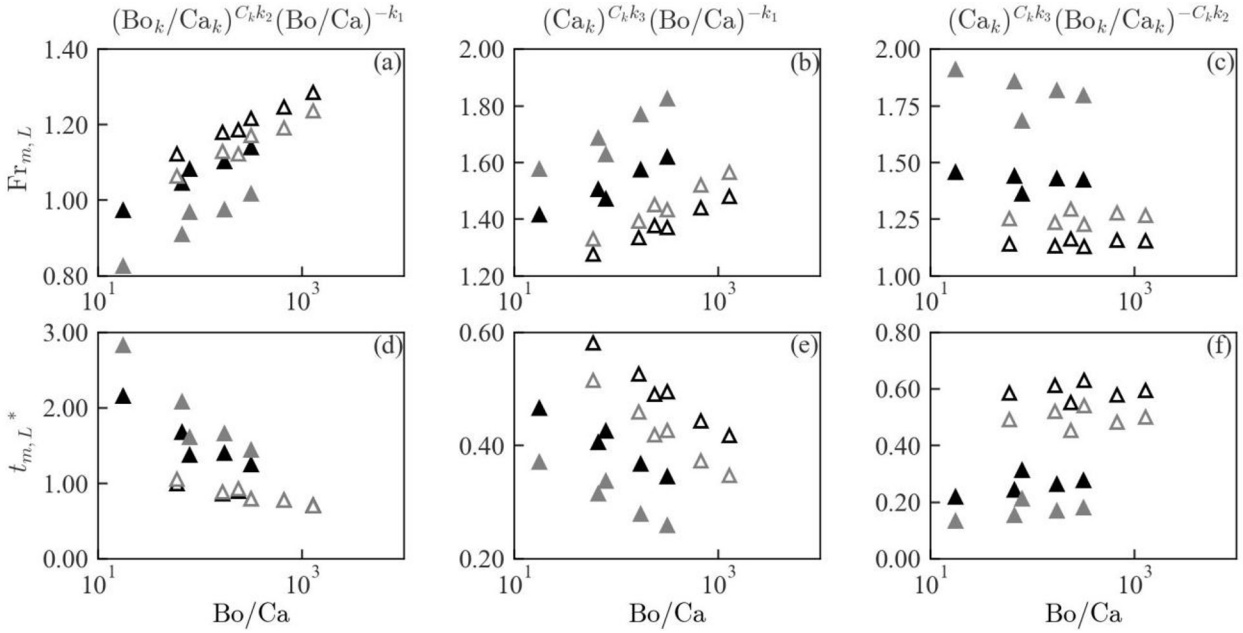

Fig. 3. Comparison of the force ratio influence for $\mathbf{Fr}_{m,L}$ and $t^*_{m,L}$ for $C_k = 0.1$ (△) and $C_k = 0.2$ (▲), and $L = d_p$ (black) and $L = H_0$ (grey).

The relative influence of grain- and kaolin-scale phenomena increases with Bo/Ca for $\mathrm{Fr}_{m,L}$ while the influence of both scales reduces with Bo/Ca for $t^*_{m,L}$. More significantly, Figure 3(b) suggests that kaolin-scale surface tension effects are more influential to $\mathrm{Fr}_{\mathrm{m,d}}$ and $\mathrm{Fr}_{\mathrm{m,H_0}}$ than the driving forces at the column scale. Furthermore, Figure 3(c) shows that for $\mathrm{Fr}_{m,L}$, kaolin-scale phenomena are more influential than grain-scale phenomena while Figure 3(f) shows that for $t^*_{m,L}$, grain-scale phenomena are more influential than kaolin-scale phenomena. Logically, these effects are exaggerated by increasing C_k.

4 Conclusions and Further work

A series of fully saturated, axisymmetric granular column collapse experiments using a fluid phase comprised of kaolin particles suspended in water were conducted to investigate the effects of a bimodal grain size distribution on acceleration phase drainage behaviour. The use of a geotechnical centrifuge allowed for a wide test parameter space where gravitational acceleration, inertial grain diameter, and the percentage of fines within the fluid phase could be varied during testing. A dimensionless parameter space consisting of 8 parameters, obtained using Buckingham's Π theorem, was postulated to characterise acceleration phase collapse dynamics. The data gathered from the current series of tests was combined with the Newtonian fluid tests from a previous study and a non-linear, least squares fitting analysis was undertaken to investigate the influence of each dimensionless parameter on the four measured quantities of interest Q: $\mathrm{Fr}_{\mathrm{m,d}}$, $\mathrm{Fr}_{\mathrm{m,H_0}}$, $t^*_{m,d}$ and t^*_{m,H_0}. As was found for the Newtonian fluid test cases, all values of Q scaled independently of each other and scaled with $Q = \left(\frac{\mathrm{Bo}}{\mathrm{Ca}}\right)^{k_1}\left(\frac{\mathrm{Bo}_k}{\mathrm{Ca}_k}\right)^{k_2 C_k}(\mathrm{Ca}_k)^{k_3 C_k}(\rho^*)^{k_4}(r^*)^{k_5}$ where k_1-k_5 are constants dependent on Q. Unlike the Newtonian fluid test case, the inclusion of kaolin particles appears to couple all Q with kaolin-scale surface tension effects which, for the range of the Bo/Ca values tested, was more influential to $\mathrm{Fr}_{\mathrm{m,d}}$ and $\mathrm{Fr}_{\mathrm{m,H_0}}$ than column-scale inertial and viscous forces. Future work involves considering the influence of a bimodal grain size distribution on the maintenance of excess pore pressures by conducting similar analyses for the dissipation of fluid pressure at the base of the column over the duration of the collapse.

References

1. B.W. McArdell, P. Bartelt, J. Kowalski. Geophys. Res. Lett. **34** (2007)
2. C.G. Johnson, B.P. Kokelaar, R.M. Iverson, M. Logan, R.G. LaHusen, J.M.N.T. Gray. J. Geophys. Res. Earth Surf **117** (2012)
3. J. Kowalski, J.N. McElwaine. J. Fluid Mech. **714** (2013)
4. R.M. Iverson, D.L. George. Proc. R. Soc. A **470** (2014)
5. F. Bouchut, E.D. Fernández-Nieto, E.H. Koné, A. Mangeney, G. Narbona-Reina. EPJ Web Conf. **140** (2017)
6. R.M. Iverson, M. Logan, R.G. LaHusen, M. Berti. J. Geophys. Res. **115** (2010)
7. R. Kaitna, M.C. Palucis, B. Yohannes, K.M. Hill, W.E. Dietrich. J. Geophys. Res. Earth Surf **121** (2016)
8. W. Webb, C. Heron, B. Turnbull. PREPRINT available at Research Square. https://doi.org/10.21203/rs.3.rs-1622762/v1 (2023)
9. E. Buckingham. Phys. Rev. **4** (1914)
10. R.M. Iverson. Geomorphology. **244** (2015)